ISSN 0023-1584, Kinetics and Catalysis, 2016, Vol. 57, No. 5, pp. 592–601. © Pleiades Publishing, Ltd., 2016.

A Comparative Study on Catalytic Performance of Modified Nanocrystalline and Microcrystalline Zeolite X for Synthesis of Cumene by Transalkylation of 1,4-Diisopropylbenzene with Benzene[1]

R. Thakur[a] and S. Barman[b, *]

[a] *School of Chemistry and Biochemistry, Thapar University, Patiala, 147004, India*
[b] *Department of Chemical Engineering, Thapar University, Patiala, 147004, Punjab, India*
**e-mail: sbarman@thapar.edu*

Received August 10, 2015

Abstract—Cumene is a commercially important product in the petrochemical industries. In isopropylation of benzene, 1,4-diisopropyl benzene (1,4-DIPB) is produced as low value by-product. This low value by-product DIPB is used to maximize the production of commercially important product cumene by transalkylation reaction. Reduction of crystal size in zeolite can increase surface area of the external surface and in this way bring about substantial changes in catalytic activity. Moreover modification with rare-earth metal enhances the acidity of zeolite. In this work, nanocrystalline and microcrystalline zeolite X were modified with cerium to study the combine effect of crystal size and ion modification of zeolite on selectivity of cumene in commercially important transalkylation reaction. Benzene and 1,4-diisopropylbenzene in a molar ratio of 1 to 12.5 were subjected to vapour-phase reaction in the temperature range of 498 to 593 K at atmospheric pressure with space time of 5.27–10.54 kg h/kmol. Nanosized crystalline zeolite gives much higher conversions of 1,4-DIPB than microcrystalline zeolite. Over cerium modified nanosized zeolite CeX_N 81.85% conversion of 1,4-DIPB and 97% cumene selectivity were achieved. It was found that stability and activity of CeX_N for cumene synthesis was much higher than that of CeX_M zeolite. Kinetic constants for the reactions were estimated and the activation energies for various reactions over CeX_M were determined. The activation enegy for transalkylation reaction was found to be 78.54 kJ/mol.

Keywords: cerium, nanosized crystalline X zeolite, transalkylation, cumene, kinetics

DOI: 10.1134/S0023158416050189

Cumene (**C**) is a commercially important product in the petrochemical industry. It is an significant component of motor fuels boiling gasoline range and showing high antiknock values. Cumene is in demand for the production of phenol, acetone, bisphenol-A, cymene and other polyalkylated hydrocarbons containing at least one isopropyl group [1–8]. Conventionally, it is produced by alkylation of benzene with propylene. However, during the alkylation process, 1,4-diisopropylbenzene (1,4-DIPB) isomers in amount of 5–10 wt % are produced as by-product. These isomers are transported to the fuel pool in many industrial plants. This results in additional raw material consumption affecting the economy of the entire process. The by-product DIPB can be utilized to produce cumene by transalkylation with benzene (B) [9, 10]. In the industry, alkylation and transalkylation can be carried out in the same reactor in the single reaction zone or using a reactor having two reaction zones in series, one for alkylation and the other for transalkylation to maximize the production of monoalkylated product cumene [11]. Hence, the transalkylation process is needed to be developed with a suitable catalyst for the commercial production of cumene. Currently, for transalkylation reactions, zeolite catalysts are used instead of conventional Friedel–Crafts catalysts. The Friedel–Crafts catalysts are highly corrosive to process equipment and are difficult to separate from the product. On the other hand, zeolites are used due to their high activity, stability, selectivity, regenerability and environment-friendly nature [12]. In the last decade, the synthesis of zeolites with small particle size has drawn attention of many researchers. It was reported that reduction of particle size from the micrometers to the nanometers brings about substantial changes in the properties of zeolites in the area of catalysis and separation [13]. Zeolite nanoparticles have large external surface area. In zeolites composed

[1] The article is published in the original.

of smaller crystallites the mean free path of a diffusing molecule is smaller than that in conventional zeolite [14–16]. A number of studies shows that zeolite catalysts are potential catalysts for transalkylating DIPB with benzene 17, 18]. However, the rate limiting step of the reactions tends to be controlled by diffusion of reactant/product molecules. Moreover, carbonaceous residue (coke) is easily formed near the external surface of the crystal under the diffusion controlled conditions whereby the pore plugging easily occurs, leading to a short lifetime of zeolite catalyst. In order to achieve a low diffusion resistance, application of nanozeolites is effective because the mean free path of diffusing molecule of a reactant and product hydrocarbons depends on the crystal size of the zeolites. Very scarce literature is available on transalkylation reaction over nanocrystalline zeolites. The surface acidity is of importance when the zeolite is intended to be used as a catalyst in reactions involving bulky molecules [16]. Zeolite containing sodium ions in its structures are inactive for transalkylation reaction. In order to generate acidity in the surface of zeolites, modification of zeolite with polyvalent cations from rare-earth metals (La, Ce, etc.) has been reported that served to prepare zeolites with superior catalytic activity [19–24]. Introduction of rare-earth metal ions increases the acidity of the zeolite catalysts and thereby enhances the reaction rates. Transalkylation reactions were carried out in the vapor phase over commercial H-mordenite catalyst in a fixed-bed down-flow reactor [25]. The commercial H-mordenite was found to be successful in transalkylation reaction. The conversion increased with increasing in benzene/DIPB ratio and temperature. The transalkylation of diisopropylbenzene with benzene was carried out over catalysts that included three acidic commercial zeolites: beta, Y and mordenite with different aluminum contents (e.g. Si/Al molar ratio) [26]. Comparing to conventional liquid phase conditions, the use of supercritical CO_2 did not result in superior catalytic transalkylation activity for the Y-zeolite. On the contrary, an important improvement in product yield was obtained with the beta and mordenite zeolites. Transalkylation reactions were carried out over SAPO-5 catalyst. The catalyst based on SAPO-5 showed very good results when loaded with a small quantity of platinum (0.005% w/w) in the transalkylation of commercial DIPB with benzene [18]. Hierarchical beta zeolite was prepared via the dry gel conversion method and its catalytic activity was compared with that of the conventional beta zeolite for transalkylation of diisopropylbenzene with benzene [27]. In this work, nanocrystalline and microcrystalline zeolite X were modified with cerium to study the effect of crystal size and metal modification of zeolite on different reaction parameters of transalkylation reaction used for the synthesis of commercially important cumene.

EXPERIMENTAL

Materials

Benzene, 1,4-DIPB, TM-40 colloidal silica, silicon dioxide, sodium hydroxide, sodium aluminate, ammonium chloride were obtained from "Sigma–Aldrich Pvt. Ltd." (India). Commercial NaX zeolite extrudates used in present study was procured from "Fresia zeolite" (Mumbai). It was in the form of 1.5 mm extrudates. Ceric ammonium nitrate used to exchange NaX with cerium salts was supplied from "CDH chemicals" (India).

Catalyst Synthesis and Modification

The nanocrystalline NaX zeolite was synthesized by hydrothermal crystallization and then modified with cerium by ion exchange method [12, 28]. For the preparation of nanocrystalline NaX, aluminate and silicate solutions were mixed together in the molar ratio 5.5 Na_2O : 1.0 Al_2O_3 : 4.0 SiO_2 : 190 H_2O. Typically, an aluminosilicate gel containing 5.34 g of NaOH, 2.42 g of $NaAlO_2$, 3.43 g of SiO_2, and 50.0 g of H_2O was prepared. Freshly prepared sodium aluminate solution and fumed silica were placed in a 250 mL plastic bottle, the silicate sources were directly mixed with freshly prepared aluminate solution at room temperature. This mixture was then immediately moved to a shaker for hydrothermal crystallization which was conducted at 333 K for 4 days at 250 rpm. The powdered products were recovered with centrifugation, washed with deionized water until pH < 8, and then dried at room temperature for 24 h. Nanocrystalline NaX (synthesized) and microcrystalline NaX (commercially available) were further modified with cerium to assess the effect of cerium ions replacing sodium ions. For modification with cerium of both the zeolites, the zeolites were refluxed with ammonium nitrate solution 363 K for 6 h. This procedure was repeated three times, thereby converting NaX zeolite into the NH_4^+X form. After each ion exchange operation the samples were heated at 623 K. The samples were then refluxed with required percentage of ceric ammonium nitrate solution at 363 K for 16 h thereby modifying the HX zeolite [29]. Finally, the samples were dried and calcined for 4 h at 623 K. In this study, microcrystalline zeolite modified with cerium, synthesized nanocrystalline zeolites modified with cerium, unmodified micro X and nano X zeolites are designated as CeX_M,CeX_N, NaX_M, and NaX_N, respectively. NaX_M zeolite was treated with 2, 5, 7, 10, and 12% cerium nitrate solutions [12]. Zeolite CeX_M exchanged with 10% cerium nitrate solution showed the maximum conversion. For this reason, all the reactions were carried out over zeolite X exchanged with 10% cerium nitrate solution.

Catalyst Characterization

From Energy-dispersive X-ray spectroscopy (EDX), Si/Al molar ratio of NaX_N was found to be 1.25 which matches well with the commercial NaX_M zeolite. The characterization of the synthesized nanozeolite is shown in the Table 1.

X-ray diffraction (XRD) of samples were performed on a PANalytical X'Pert Pro Diffractometer in the $5° \le 2\theta \ge 40°$ range using CuK_α radiation. The XRD patterns of the nanozeolite and cerium exchanged zeolites (Fig. 1) were almost identical to that of the sodium form of microsized zeolite. On close inspection of XRD data it was observed that peak intensity in nanosized and cerium modified nanozeolite decreases. A very slight shift in XRD 2θ values was noticed in nanosized and cerium modified nanozeolites. The decrease in intensity in case of nanozeolite is due to decreasing crystal size whereas in case of cerium modified nanozeolite a further decrease in intensity of peaks is due to some loss of crystallinity due to addition of metal ions. Diffraction lines corresponding to metal oxide were observed in case of cerium modified zeolites. As cerium exchange of zeolite is carried out using high concentration of ceric ammonium nitrate solution, the excess cerium can be deposited on a zeolite leading to formation of metal oxide. The peaks at 6.19° (111), 11.6° (311), 18.6° (511), 20.3° (440) and 23.5° (533) correspond to NaX faujasite zeolite topology. However, the additional peaks observed on the diffractograms of cerium exchanged nanosized zeolite and undetected in unmodified zeolites were due to cerium oxide. The unit cell paremeters of NaX zeolite are $a = 24.74$ Å and $\alpha = \beta = \gamma = 90°$. The height of the strongest peak at 6° (2θ) was taken as a measure of crystallinity. The extent of crystallinity was estimated by comparing the X-ray diffraction peak height at 6° (2θ) for the modified sample to the original peak height at 6° (2θ) for the unmodified microsized zeolite (commercial sample).The extent of zeolite crystallinity the prepared nano NaX_N zeolite was calculated using the following equation:

Crystallinity, % = (peak height at 6° of nanozeolite) × 100/(peak height at 6° of standard material).

The crystallinity of the nano NaX_N and nano CeX_N were found to decrease compared to their microsized analogues.

Scanning electron microscopic (SEM) images were recorded using JEOL JSM-6510LV SEM equipment (JEOL). SEM images of synthesized nanocrystalline NaX and cerium modified nanocrystalline NaX show that the particles were oval or rounded in shape. The average particle size of nanocrystalline zeolite was found to be ~500 nm. Moreover, there was no structural change observed in nanocrystalline NaX zeolite modified by cerium. Ammonia temperature programmed desorption (TPD) of the parent and modified catalysts were performed in a CHEM-BET 3000 instrument (Quantachrome). Catalyst sample (0.1 g) was first degassed at 723 K for 1 h with nitrogen followed by cooling to 273 K temperature. Nitrogen–ammonia gas (1 mol %) mixture was then passed through the sample for 1 h. The catalyst sample was heated to 372 K until the steady state was attained; thereafter the temperature of the sample was raised up to 1173 K at a heating rate of 10 degree/min. The amount of desorbed ammonia was detected by a Thermal conductivity detector (TCD) analyzer. Temperature programmed desorption profile of ammonia was studied with NaX_M, CeX_M, NaX_N and CeX_N zeolites (Fig. 2). The profiles show that the catalysts contain mainly two types of acid sites of different strengths. Low temperature peak is due to ammonia desorption from the weak acid sites, whereas, the peak at higher temperature is due to the desorption of strongly adsorbed ammonia from strong acid sites. TPD profiles show that the acidity of microcrystalline and nanocrystalline zeolite is almost similar. The strength of the acid sites increases with cerium exchange of

Table 1. Characteristics of different zeolites used for 1,4-DIPB transalkylation

Composition, wt %	NaX_M	NaX_N	CeX_M	CeX_N
SiO_2	48.26	48.67	50.76	54.3
Al_2O_3	31.87	31.75	32.02	34.2
Fe_2O_3	3.17	0	2.42	0
Na_2O	15.67	19.58	0.80	2.20
CeO_2	0	0	14.00	9.30
K_2O	0.07	0	0	0
BET surface area, m^2/g	478	633.6	370	530
Acidity, meq/g of catalyst	0.25	0.28	1.27	1.35

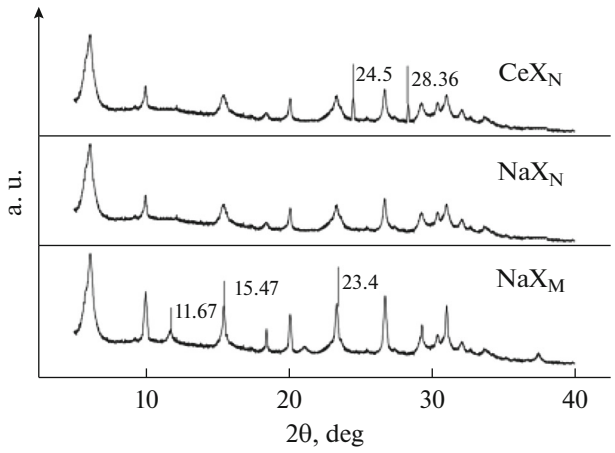

Fig. 1. XRD of NaX and CeX zeolites.

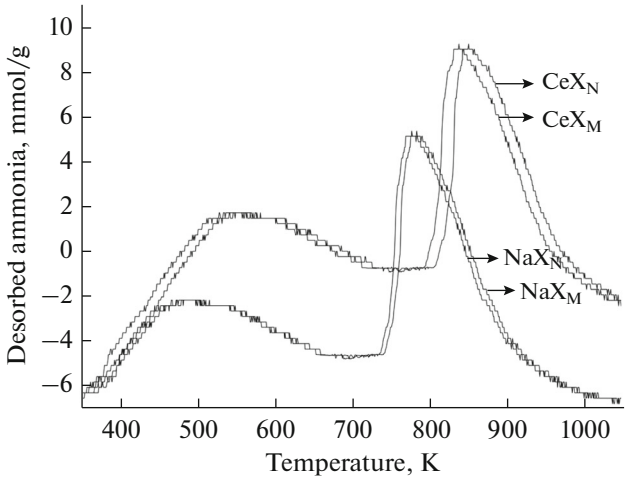

Fig. 2. TPD of NaX and CeX zeolites.

zeolites as the peak area increases with Ce exchange. Thus, it can be concluded from the Fig. 2 that cerium exchange leads to increase in acidity of zeolite. The acidity of various zeolites has been reported in Table 1.

Experimental Procedure and Product Analysis

Transalkylation of 1,4-DIPB with benzene was carried out in a fixed-bed, continuous down-flow, stainless steel (SS 316) reactor connected with a preheater in the upstream and a condenser at the outlet. About 2 g of zeolite was loaded into the reactor with the support of wire mesh and the temperature was measured by a thermocouple placed in a thermowell extending from the top of the reactor to the centre. Prior to the experimental runs catalyst were activated for 3 h in the flowing nitrogen. The mixture composed of 1,4-DIPB and benzene was fed into the reactor with the help of a dosing pump. After the completion of the reaction, the product vapor and the unreacted reactants were collected in a condenser and the liquid samples were collected and analyzed by a Gas chromatograph ("Bruker", capillary column: 10 m × 0.53 mm × 1.5 μm) using a Flame ionisation detector (FID). The conversion of 1,4-DIPB and selectivity of cumene and 1,3-DIPB was calculated according to following formula:

$$\text{1,4DIPB conversion} = \frac{(\text{1,4DIPB in Feed-1,4DIPB in product mixture})}{(\text{1,4DIPB in feed})} \times 100$$

$$\text{Cumene Selectivity} = \frac{(\text{Cumene in the product mixture})}{(\text{aromatics in product excluding 1,4DIPB and Benzene})} \times 100$$

$$\text{1,3DIPB Selectivity} = \frac{(\text{1,3DIPB in the product mixture})}{(\text{aromatics in product excluding 1,4DIPB and Benzene})} \times 100$$

RESULTS AND DISCUSSION

Effect of Cerium Loading on Conversion of 1,4-DIPB

Commercially available NaX_M zeolites were treated to exchange its sodium ions with cerium ions [12]. A series of zeolites were prepared by ion exchange with varying concentration of ceric ammonium nitrate solution. The prepared cerium exchanged zeolite contained 1.34, 4.02, 5.3, 7.8, and 10.89% cerium respectively. The experiments were carried out to find the effect of cerium loading in zeolite on conversion and selectivity. In Fig. 3, it is seen that the DIPB conversion and cumene selectivity both increase with an increasing cerium content in the NaX_M zeolite. This is due to the strong acid site generated at the higher level of exchange [12]. CeX_M contained 10.89% cerium shows the highest conversion (71.87%). However, selectivity of cumene over this catalyst was lower than with the zeolite loaded with 7.8% cerium. Therefore, all the reactions were carried out over CeX_M containing 7.8% cerium. For comparison NaX_N zeolite was also modified with a 10% cerium nitrate solution and tested in the reactions.

Time-on-stream Behavior

The stability of NaX_M, CeX_N and CeX_M zeolite was assessed using time-on-stream of about 3 h at 553 K and atmospheric pressure (Fig. 4). In the presence of CeX_N zeolite 81.4% conversion of 1,4-DIPB was achieved whereas 71% conversion of DIPB was achieved over CeX_M under the same reaction conditions. It is seen that after 3 h time-on-stream, CeX_N zeolite is more stable than CeX_M zeolite. With increasing time, deactivation of catalyst occurs due to the blockage of pores with the reactants and products. As the time-on-stream increases, 1,4-DIPB conversion over CeX_M decreases by 5.77% whereas in case of CeX_N zeolite there was only 1.6% decrease in conversion after 3 h. A higher conversion of DIPB in case of nanozeolite was due to a larger external surface area and also to a larger number of active sites present in the external surface which oppose the deactivation of zeolite. CeX_N zeolite catalyst preserves stability under these reaction conditions.

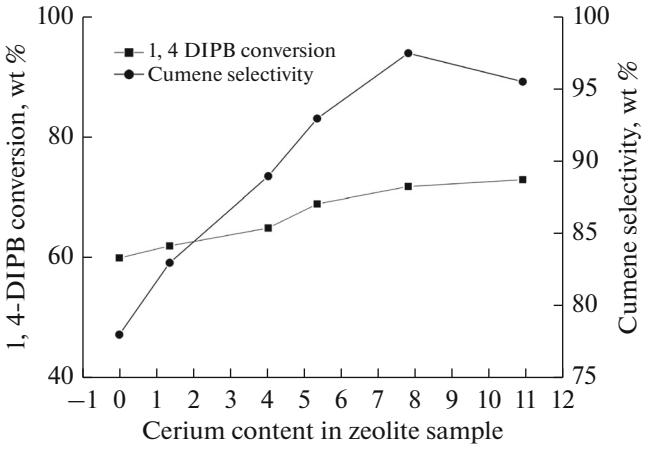

Fig. 3. Effect of cerium concentration on 1,4-DIPB conversion and cumene selectivity over CeX_M. Reaction conditions: pressure 1 atm, temperature 553 K, space-time 10.54 kg h/kmol, mole ratio of benzene : 1,4-DIPB = 7.5 : 1, N_2 to feed ratio 0.2.

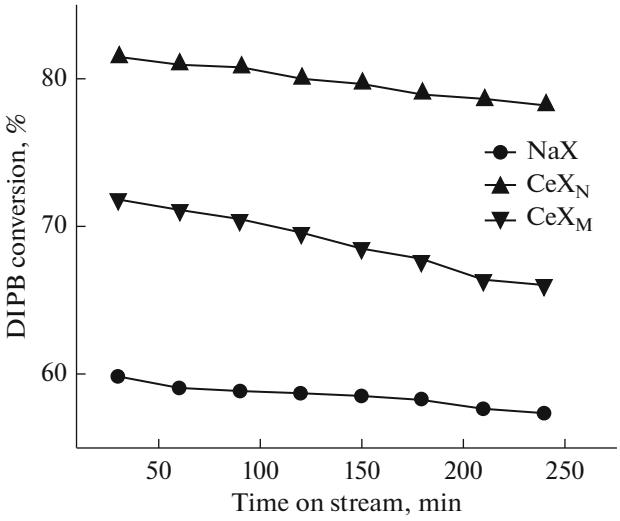

Fig. 4. Time-on-stream behavior of different zeolite catalysts. Reaction conditions: pressure 1 atm, temperature 553 K, space-time 10.54 kg h/kmol, mole ratio of benzene: to 1,4-DIPB = 7.5 : 1, N_2 to feed ratio 0.2.

Effect of Reaction Temperature on Conversion of 1,4-DIPB and Product Selectivity

The catalytic performance of CeX_M and CeX_N zeolite at different temperatures is shown in Fig. 5. The figure shows that at lower temperature 513 K, conversion of 1,4-DIPB over both the catalysts was nearly comparable. With increasing temperature, conversion of 1,4-DIPB increases up to 81.51% at 553 K over CeX_N zeolite. The highest conversion of 1,4 DIPB over CeX_M zeolite at 573 K (76.06%) was comparable to 76.9% conversion of 1,4-DIPB over CeX_N zeolite at the same temperature. A higher conversion over CeX_N zeolite is due to a higher external surface area and an enhanced concentration of active sites on the catalyst surface. The decrease in conversion of 1,4-DIPB with a further increase in temperature may be due to the formation and deposition of coke on the active sites. Cumene selectivity increases with increasing temperature. At 573 K cumene selectivity was 97.98% but at higher temperature, selectivity of cumene decreases significantly to 93.4% over CeX_N zeolite due to the formation of other side products. Product distribution of transalkylation reactions over different zeolite catalyst at 553 K is shown in Table 2.

Effect of Reactant Ratio on Conversion of 1,4-DIPB and Product Selectivity

To investigate the effect of reactant ratio on 1,4-DIPB conversion and cumene selectivity, the benzene to 1,4-DIPB ratio was varied from 1–12.5. At reactant ratio of 7.5, conversion of 1,4-DIPB over CeX_M was 71.87 and 81.51% coversion of 1,4-DIPB was achieved over CeX_N. It can be seen from the Fig. 6 that the conversion increases with increase in reactant ratio over both the zeolites. With the increase in reactant ratio, 1,4-DIPB conversion increases and reaches maximum at the ratio of 7.5 above which conversion of 1,4-DIPB decreases due to a lower availability of the limiting reactant. Smaller benzene molecules can easily enter the pores of zeolites and their concentration at external surface is not high enouth for the reaction to occur. Since increased benzene to 1,4-DIPB ratio is required for high 1,4-DIPB conversion, it appears that at higher benzene to 1,4-DIPB ratio, benzene mole-

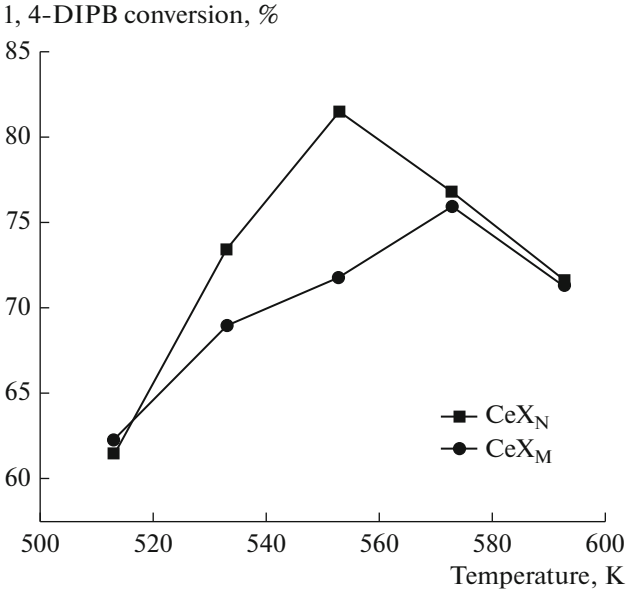

Fig. 5. Effect of reaction temperature on DIPB conversion over CeX_M and CeX_N. Reaction conditions: pressure 1 atm, space-time 10.54 kg h/kmol, mole ratio of benzene : 1,4-DIPB = 7.5 : 1, N_2 to feed ratio 0.2.

cules are present in large amounts both in the pore volume and at the external surface. Accordingly, this favours the interaction between benzene and 1,4-DIPB. However, with a further increase in benzene/DIPB ratio benzene molecules will compete with 1,4-DIPB molecules for adsorption sites. Accordingly, lower occupancy of active sites by 1,4-DIPB molecules leads to decreased 1,4-DIPB conversion. In the presence of CeX_M selectivity of cumene was found to be 97.08% at a mole ratio of 1 and it decreased to 91.92% at a mole ratio was increased to 12.5. In the case of nanozeolite selectivity of cumene decreases from 97.93% at a mole ratio of 1 and further to 73.6% at a mole ratio 12.5. Decrease of cumene selectivity at a higher mole ratio is due to the enhanced formation of side products, 1,3-DIPB and *n*-propylbenzene.

Effect of Space-Time Conversion of 1,4-DIPB and Product Selectivity

The effect of space-time on conversion of 1,4-DIPB and selectivity of cumene was investigated in the range of 5.27–10.54 kg h/kmol with the results shown in the Fig. 7. Conversion of 1,4-DIPB increases with increasing space-time as evident from the data obtained over catalysts CeX_M and CeX_N. This is due to the fact that increasing contact time intensifies the interaction of reactant molecules with the surface of the catalyst. At higher contact time, the feed molecules remained in contact with the catalyst particle for longer time thus increasing the number of reactants that could be converted into products. In the case of nanozeolite it was found that with increasing space time the selectivity of cumene increased from 92.41 to 96.64% whereas for the CeX_M zeolite, selectivity of cumene remains nearly constant (98–97.54%) resulting in the formation of side product 1,3-DIPB and *n*-propyl benzene. The product distribution over different catalysts found at a space-time of 7.908 kg h/kmol is shown in Table 3.

Mass Transfer Considerations

Based on the product distribution, it is evident that the selectivity of cumene is higher over CeX_M than on CeX_N zeolite. Kinetic modelling was done for the reaction over CeX_M zeolite. The kinetic runs were carried out in the region of the mass transfer free resistances. For gas–solid heterogeneous reactions, this resistance may be external or internal, within the catalyst particles. Experiments were carried out to estimate the external diffusional effects varying feed rates and catalyst size remaining constant space-time. The results shown in Table 4 indicate that the conversions of 1,4-DIPB at a constant space velocity are independent of feed rate. Therefore, the external mass transfer resistance is negligible. Experiments were carried out to investigate the effect of intraparticle diffusion by varying the catalyst particle size at a constant space-time. The experimental data are presented in the Table 5. It is seen that there was no change in conversion of 1,4-DIPB with catalyst size which indicates negligible intraparticle mass transfer resistance in the particle size range studied. The kinetic study was performed within the intraparticle diffusion free range.

Table 2. Product distribution at 553 K over different catalysts

Product distribution, wt %	NaX_M	CeX_M	CeX_N
Aliphatics	0.010	0.013	0.141
Benzene	75.34	71.31	67.694
Toluene	0.127	0.160	0.050
Xylene	0.075	0.086	0.109
Cumene	14.99	21.67	27.116
n-Propylbenzene	0.032	0.041	0.025
C_{10}	0.011	0.024	0.034
1,3-DIPB	0.181	0.221	0.481
1,4-DIPB	9.234	6.468	4.251
1,4-DIPB conv., wt %	59.85	71.87	81.51

Reaction conditions: pressure 1 atm, space-time 10.54 kg h/kmol, mole ratio of benzene : 1,4-DIPB = 7.5 : 1, N_2 to feed ratio 0.2.

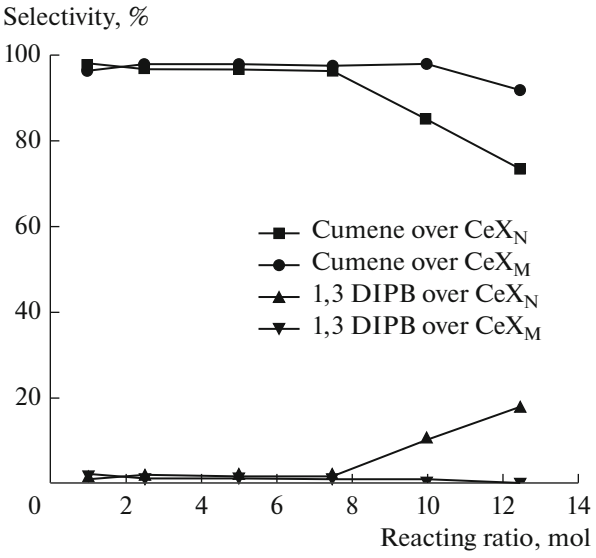

Fig. 6. Effect of reactant mole ratio on product selectivity over CeX_M and CeX_N. Reaction conditions: pressure 1 atm, temperature 553 K, space-time 10.54 kg h/kmol, N_2 to feed ratio 0.2.

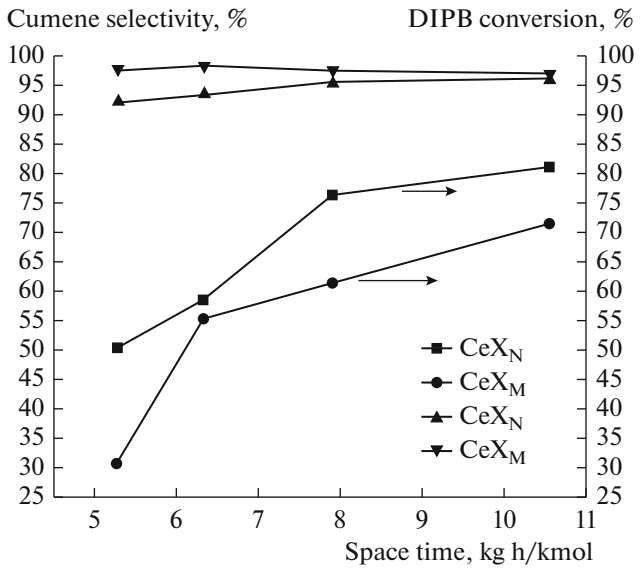

Fig. 7. Effect of space-time on product selectivity and 1,4-DIPB conversion over CeX_M and CeX_N. Reaction conditions: pressure 1 atm, temperature 553 K, mole ratio of benzene : 1,4-DIPB = 7.5 : 1, N_2 to feed ratio 0.2.

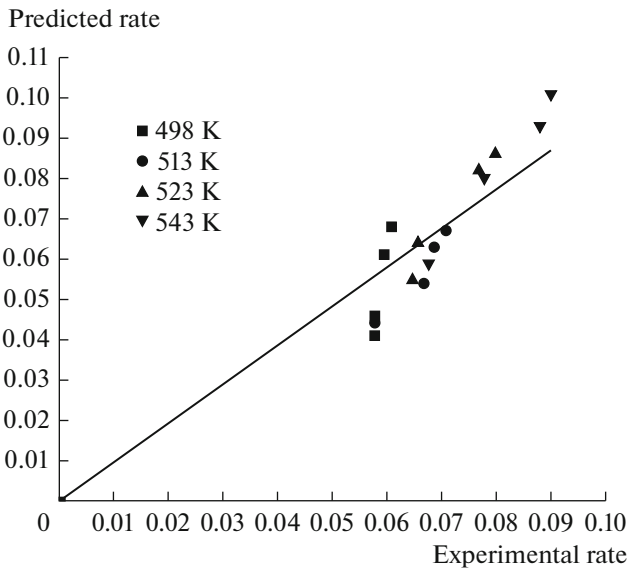

Fig. 8. Experimental *vs* predicted rates of transalkylation reaction.

Kinetic Modelling

The kinetic runs were carried out at four different temperatures and the results are shown in Fig. 8. The experiments were carried out to choose the zone, in which mass transfer effects were negligible. In accordance with the product distribution, the system can be described by the following reaction scheme. Transalkylation of 1,4-DIPB with benzene is a complex reaction which is accompanied by the following reactions.

$$\text{1,4-DIPB transalkylation: 1,4-DIPB} + \text{Benzene} \xrightarrow{k1} \text{2-Cumene} \quad \text{(I)}$$

$$\text{Isomerisation: 1,4-DIPB} \xrightarrow{k2} \text{1,3-DIPB} \quad \text{(II)}$$

$$\text{Disproportionation: 1,4-DIPB} \xrightarrow{k3} \text{Benzene} + \text{Aliphatics} \quad \text{(III)}$$

$$\text{Benzene} + \text{Aliphathics} \xrightarrow{k4} C_8 + C_{10} \quad \text{(IV)}$$

Scheme.

With the help of the above reaction scheme, various reaction rate models (adsorption, desorption, and surface reaction controlling) were formulated following Langmuir–Hinshelwood approach. The models were tested with the help of the experimental data. All models, except that involving a surface controlled reaction, gave negative constants. Hence they were not considered. Using the rate of disappearance of 1,4-DIPB, an attempt was made to fit Langmuir–Hinshelwood–Hougen–Watson model to the kinetic data. As it can be seen from the product distribution, aliphatics and C_{10} are produced in negligible amount. Therefore to avoid the complexity in the model, these reactions were neglected in preparing the model equations. Given also that cumene adsorption on active site is very weak cumene adsorption factor can also be neglected [18].

Dual-site mechanism:

$$-r_{\text{DIPB}} = [k_1 k_{\text{B}} k_{\text{DIPB}}\, p_{\text{B}}\, p_{\text{DIPB}} + (k_2/C_{\text{v}}) k_{\text{DIPB}}\, p_{\text{DIPB}}] C_{\text{v}}^2 \quad (1)$$

where

$$C_{\text{v}} = \frac{1}{(1 + k_{\text{B}} p_{\text{B}} + k_{\text{DIPB}} p_{\text{DIPB}})}$$

Single-site mechanism:

$$r_{\text{DIPB}} = [k_1 k_{\text{DIPB}} p_{\text{B}} p_{\text{DIPB}} + k_2 k_{\text{DIPB}} p_{\text{DIPB}}] C_{\text{v}}, \quad (2)$$

where

Table 3. Product distribution at space-time 7.908 kg h/kmol over different catalysts

Product distribution, wt %	NaX_M	CeX_M	CeX_N
Aliphatics	0.001	0.002	0.142
Benzene	76.06	72.361	73.03
Toluene	0.043	0.085	0.043
Xylene	0.041	0.074	0.081
Cumene	12.049	18.556	20.732
n-Propylbenzene	0.011	0.037	0.026
C_{10}	0.007	0.019	0.022
1,3-DIPB	0.078	0.198	0.571
1,4-DIPB	11.76	8.8	5.354
1,4-DIPB conv., wt %	48.86	61.70	76.72

Reaction conditions: pressure 1 atm, temperature 553 K, space-time 7.908 kg h/kmol, mole ratio of benzene : 1,4DIPB = 7.5 : 1. N_2 to feed ratio 0.2.

Table 4. Effect of external diffusional resistances on conversion of DIPB over CeX_M

Space-time, kg h/kmol	Conversion of DIPB, %	
	catalyst weight, kg	
	0.002	0.004
5.75	46.01	46.79
6.3	49.32	49.92
7.9	60.18	60.87

Reaction conditions: pressure 1 atm, temperature 553 K, mole ratio of benzene : 1,4-DIPB = 7.5 : 1, N_2 to feed ratio 0.2.

$$C_v = \frac{1}{(1 + k_{DIPB}p_{DIPB})}$$

Stoichiometric model:

$$-r_{DIPB} = k_1 p_B p_{DIPB} + k_2 p_{DIPB} \quad (3)$$

The partial pressure (p) of 1,4-DIPB and benzene are related to the fractional conversions and the total pressure (P) by these following equations :

$$p_{DIPB} = (1 - X_{DIPB})P/10.2 \quad (4)$$

$$p_B = (7.5 - X_B)P/10.2 \quad (5)$$

$$p_C = X_C/10.2 \quad (6)$$

where the total number of moles in the reaction is 10.2. A non-linear regression algorithm was used for parameter estimation. The kinetic parameters in the three models were estimated by the least square method based on the error function. The minimization of the error function in respect with the unknown parameters of the three kinetic models was performed by the Levenberg–Marquardt method [30].

Table 5. Effect of intraparticle diffusional resistance on DIPB conversion over CeX_M

Particle size, mm	Conversion of DIPB, %		
	space-time, kg h/kmol		
	5.75	6.3	7.9
0.50	47.98	51.01	61.78
1.00	47.12	51.86	60.97
1.50	46.01	49.32	60.18

Reaction conditions: pressure 1 atm, temperature 553 K, mole ratio of benzene : 1,4-DIPB = 7.5 : 1, N_2 to feed ratio 0.2.

Table 6. Estimated kinetic and adsorption parameters for reactions over CeX_M at different temperatures (Eq. 1)

T, K	Kinetic and adsorption parametrs			
	k_1	k_2	K_{DIPB}	K_B
	kmol kg^{-1} h^{-1}		atm^{-1}	
498	2.58	1.04	1.49	2.50
513	4.83	2.03	0.83	2.20
533	8.04	4.59	0.53	1.80
553	17.64	8.14	0.26	0.31

Model Discrimination

By using the values of the constants for model equation 1 as shown in Table 6, the standard error in estimating the rate of disappearance of 1,4-DIPB was determined to be 3.10×10^{-4}. For model equation 2, the standard error was found to be 7.8×10^{-3}. For model equation 3, the standard error was estimated to be 2.6×10^{-3}. By comparing the standard errors, model equation 1 was considered to be the best kinetic model among the three models used to represent the reaction system under investigation. The experimental and the predicted 1,4-DIPB conversions from equation 1 at four different temperatures are plotted in Fig. 8. The figure shows that the proposed reaction rate expression predicts the 1,4-DIPB conversion values comparable with those found in the experiments. The kinetic constants evaluated and tabulated at various temperatures (Table 6) were used to determine the activation energy and frequency factor using Arrhe-

nius relationships. Activation energy for both reactions were calculated using following equation

$$\ln K = \ln A - E_a/RT \quad (7)$$

A value of the activation energy for transalkylation reaction was found to be 78.54 kJ/mol which was similar to estimate for the same type of reactions over zeolites obtained by other investigators [18, 25, 26, 31]. Activation energies of 109 and 110 kJ/mol calculated for reactions proceeding in the temperature range of 383–419 K on X zeolites were reported [26]. Similar values were also derived from experiments with 13X zeolite and mordenite [18, 27] in isopropyl alcohol dehydration.

CONCLUSIONS

Nanocrystalline zeolite (NaX_N) was successfully synthesized with an average crystal size of 500 nm, 90% crystallinity and surface area of 633 m^2/g. This nanocrystalline zeolite was further modified with cerium ions to assess the effect of crystal size and ion exchange on acidity and activity of the catalyst. Time-on-stream study shows that CeX_N zeolite exhibits much higher conversion and stability than CeX_M treated with 10% cerium nitrate solution. As high as 81.85% of 1,4-DIPB with cumene selectivity of 97% was converted over nanozeolite CeX_N whereas 71% conversion of 1,4-DIPB and 98% cumene selectivity were achieved over CeX_M. From the experimental results presented above it can be concluded that crystal size and acidity significantly affect activity and selectivity. A kinetic model was proposed for the reactions and the parameters of the model equation were estimated. A good correlation was obtained between experimentally found and predicted rate. Based on the kinetic rate model, further scale up of the reactor can be suggested. From the estimated kinetic constant, the apparent activation energy for 1,4-DIPB transalkylation reaction was determined to be 78.54 kJ/mol and apparent activation energy for isomerisation reaction was found to be 84.56 kJ/mol.

ACKNOWLEDGMENTS

One of the authors, S. Barman is thankful to Department of Science and Technology, New Delhi, India for funding the grant during the tenure of this work.

NOTATION

B	Benzene
C	Cumene
Ce	Cerium
CeX_N	Cerium modified nanocrystalline zeolite X
CeX_M	Cerium modified microcrystalline zeolite X
NaX_N	Nanocrystalline zeolite X
DIPB	Diisopropyl benzene
k_1–k_4	Kinetic constants, kmol kg^{-1} h^{-1}
K_B	Adsorption constant for benzene, atm^{-1}
K_{DIPB}	Adsorption constant for DIPB, atm^{-1}
K_C	Adsorption constant for cumene, atm^{-1}
P	Total pressure, atm
p_{DIPB}	Partial pressure of DIPB, atm
p_B	Partial pressure of benzene, atm
p_C	Partial pressure of cumene, atm

REFERENCES

1. Ercan, C.F., Dautzenberg, M., Yeh, C.Y., and Barner, H.E., *Ind. Eng. Chem. Res.,* 1998, vol. 37, p. 1724.
2. Eur. Patent Appl. EP 629599 A1, 1994.
3. Medina-Valtierra, J., Zaldivar, O., Sánchez, M.A., Montoya, J.A., Navarrete, J., and Reyes, J.A., *Appl. Catal., A,* 1998, vol. 166, p. 387.
4. Barman, S., Pradhan, N.C., and Maity, S.K., *Chem. Eng. J.,* 2005, vol. 114, p. 39.
5. Geatti, A., Lenarda, M., Storaro, L., Ganzerla, R., and Perissinotto, M.J., *J. Mol. Catal. A: Chem.,* 1997, vol. 121, p. 111.
6. Meima, G.R., *CATTECH,* 1998, vol. 2, p. 5.
7. Eur. Patent Appl. EP 1949227 A1, 1999.
8. Reddy, K.S.N., Rao, B.S., and Shiralkar, V.P., *Appl. Catal., A,* 1993, vol. 95, p. 53.
9. Pradhan, A.R. and Rao, B.S., *Appl. Catal., A,* 1993, vol. 106, p. 143.
10. Suresh, R., Rajadhyaksya, A.R., and Kumbhar, P.S., *J. Chem. Technol. Biotechnol.,* 1995, vol. 62, p. 268.
11. Lei, Z., Li, C., Li, J., and Chen, B., *Sep. Purif. Technol.,* 2004, vol. 34, p. 265.
12. Barman, S. and Pradhan, N.C., *Ind. Eng. Chem. Res.,* 2005, vol. 44, p. 7313.
13. Khalil, K.J., *J. Colloid Interface Sci.,* 2007, vol. 315, p. 562.
14. Schmidt, I., Madsen, C., and Jacobsen, C.J.H., *Inorg. Chem.,* 2000, vol. 39, p. 2279.
15. Chauhan, Y.P. and Talib, M., *Sci. Rev. Chem. Commun.,* 2012, vol. 2, p. 12.
16. Naidu, K.G.S., Maity, S., Pradhan, N.C., and Patwardhan, A.V., *CHEMCON-2006,* Ankleshwar, Gujarat, India, 2006, p. 23.
17. US Patent 4375574, 1983.
18. Kodamudi, K. and Upadhyula, S., *J. Chem. Technol. Biotechnol.,* 2008, vol. 83, p. 699.
19. Rabo, J.A., Pickert, P.E., Stamires, D.N., and Boyle, J.E., *Chem. Abstr.,* 1961, vol. 55, p. 652.
20. Venuto, P.B., Hamilton, L.A., Landis, P.S., and Wise, J.J., *J. Catal.,* 1966, vol. 5, p. 81.
21. Rabo, J.A., Angell, C.L., and Schomaker, V., *Proc. 4th int. Congr. on Catalysis,* Moscow, 1968, p. 96.

22. Hunter, F.D. and Scherzer, J., *J. Catal.,* 1971, vol. 20, p. 246.
23. Mirzabekova, S.R., Dorogochinskii, A.Z., and Mortikov, E.S., *Chem. Technol. Fuels Oil,* 1977, vol. 13, p. 840.
24. Haag, W.O., Lago, R.M., and Weisz, P.B., *Nature,* 1984, vol. 309, p. 589.
25. Sotelo, J.L., Calvo, L., Pérez-Velázquez, A., Cavani, F., and Bolognini, M.A., *Appl. Catal., A,* 2006, vol. 312, p. 194.
26. Bozga, G., Lupascu, M., Zaharia, E., and Malacea, R., *12th Romanian Int. Conf. on Chemistry and Chemical Engineering,* Bucharest, 2001, p. 344.
27. Yang, H., Liu, Z., Gao, H., and Xie, Z., *Appl. Catal., A,* 2010, vol. 379, p. 166.
28. Mahdi, F. and Abdolreza, A., *Int. J. Ind. Chem.,* 2011, vol. 2, p. 140.
29. Plank, C.J., Rosinski, E.J., and Hawthorne, W.P., *Ind. Eng. Chem. Res.,* 1964, vol. 3, p. 165.
30. Press, W.H., *Numerical Recipes in Pascal,* Cambridge: Cambridge Univ. Press, 1986.
31. Forni, L., Cremona, G., Missineo, F., Bellusi, G., Perego, C., and Pazzuconi, G., *Appl. Catal., A,* 1995, vol. 121, p. 261.